J Nanostruct 16(4): 5274-5286, Autumn 2026

RESEARCH PAPER

Shell Time and Metal Type Dependent Nonlinear Optical Properties of Iron-based Core/Shell Nanostructures Synthesized by Pulsed Laser Ablation in Liquid

Fatimah M. Abdulamer, Ahmed K. Kodeary *

Department of Laser Physics, College of Science for Women, University of Babylon, Hilla, Iraq

ARTICLE INFO

Article History:
Received 28 May 2026
Accepted 05 September 2026
Published 01 October 2026

Keywords:
Core/shell nanostructures
Fe nanoparticles
Nonlinear refractive index
PLAL technique
Shell thickness

ABSTRACT

Engineering nonlinear optical (NLO) behavior of nanomaterials is a crucial prerequisite for enhancing contemporary photonic systems and optical limiting devices. This work presents a systematic investigation into the synthesis and structure-dependent optical nonlinearities of iron-based core/shell nanostructures. Specifically, the iron nanoparticles (Fe NPs) were successfully coated with transition-metal shells of varying thicknesses, namely nickel (Ni), copper (Cu), and cobalt (Co), designated as Fe@Ni, Fe@Cu, and Fe@Co nanostructures using pulsed laser ablation in liquid (PLAL) technique. The ablation process is performed in deionized distilled water (refractive index of 1.33) to create the core/shell nanostructures, using 4 minutes for the core and 2-4 minutes for the shell. Utilizing the single-beam Z-scan technique under high-intensity laser irradiation at a wavelength of 532 nm, the nonlinear refractive index (n_2), and the real part of third-order nonlinear optical susceptibilities Re($\chi 3$) were thoroughly evaluated. The experimental findings reveal that both the composition of the outer shell and its physical thickness play critical functions in tuning the NLO responses. Interfacial electronic coupling and localized surface plasmon resonance (LSPR) tuning induced significant changes in the optical nonlinearity of the core/shell nanosystems as the shell dimensions evolved. These insights offer an effective pathway for tailoring advanced, Fe-core nanostructures with optimized optical limiting and switching capabilities for optoelectronic applications.

How to cite this article
Abdulamer F., Kodeary A. Shell Time and Metal Type Dependent Nonlinear Optical Properties of Iron-based Core/Shell Nanostructures Synthesized by Pulsed Laser Ablation in Liquid J Nanostruct, 2026; 16(4):5274-5286. DOI: 10.22052/JNS.2026.04.064

INTRODUCTION

Within modern photonics and optoelectronics, the development of advanced materials with robust nonlinear optical (NLO) behaviors remains an important technological endeavor. Nonlinear optical phenomena-such as optical limiting, saturable absorption, and degenerate four-wave mixing establish the foundation for high-speed optical switching, signal processing, and the shielding of sensitive optical sensors against strong laser radiation. Therefore, designing nano-scale architectures capable of manipulating light at high intensities with high efficiency is widely investigated [1,2].

Among different nanostructures, transition metal nanoparticles have attracted significant

* *Corresponding Author Email: ahmed.kodeary88@uobabylon.edu.iq*

attention due to their unique Localized Surface Plasmon Resonance (LSPR) phenomena, which strongly govern their linear and nonlinear optical responses [3-5]. Iron nanoparticles (Fe NPs), particularly, display remarkable magnetic and electronic characteristics, rendering them exceptionally attractive for multifunctional technological applications [6]. However, bare Fe NPs often exhibit chemical instability, such as rapid oxidative process, agglomeration, and weakened environmental resistance, and possess intrinsic limitations in engineering their optical nonlinearities precisely [7,8]. To overcome these challenges, core/shell nanostructures design has emerged as a powerful and versatile strategy [9].

Utilizing the encapsulation an active metallic core embedded in a secondary metallic shell, investigators can synergistically combine the properties of both materials while simultaneously safeguarding the core from environmental degradation [10]. The choice of the shell material-specifically transition metals like nickel (Ni), copper (Cu), and cobalt (Co) introduces fascinating interfacial electronic coupling effects and modifies the local electromagnetic field surrounding the Fe core [11,12]. This interfacial hybridization significantly changes the state density and regulates the linear and nonlinear optical parameters [13].

Significantly, experimental paradigms demonstrate that these optical enhancements are highly sensitive to the physical dimensions of the nanostructure [14]. Whereas several studies have investigated core/shell nanostructures [15-18], a systematic, comparative investigation regarding how changing the shell thickness of different transition metals (Ni, Cu, and Co) regulates the NLO behavior of the Fe core remains scarce.

Tackling this crucial knowledge gap, the ongoing research aims to methodically synthesize, characterize, and evaluate the thickness-dependent NLO properties of Fe@Cu, Fe@Ni, and Fe@Co core/shell nanostructures. By utilizing advanced characterization techniques and non-linear optical measurements (such as the Z-scan technique), this work explains the correlation between shell thickness, interfacial interactions, and the resulting NLO coefficients. The findings of this research provide a reliable blueprint for designing highly tunable, Fe-based core/shell nanostructures tailored for optical limiting applications and high-performance photonic technologies.

Nonlinear optics (NLO) is defined as the field that deals with the interaction of high intensity light propagating through transparent optical materials; this interaction induces a change in the nonlinear optical parameters of these materials. The nonlinearity parameters of transparent media, such as the nonlinear refractive index (n_2), the nonlinear absorption coefficient (β), and the third-order nonlinear susceptibilities (χ3) can be measured using several techniques. Among these, the Z-scan technique is widely recognized as a highly sensitive and straightforward single-beam method for evaluating nonlinear optical parameters with a strong emphasis on third-order optical nonlinearities. In addition, it is a simple, inexpensive, and highly effective tool [19,20].

The Z-scan technique can be conducted in two distinct arrangements depending on the presence of an aperture positioned in the propagation path of the laser beam, carefully placed in front of the photo-detector. Omission of an aperture establishes the open-aperture (OA) Z-scan mode, whereas utilizing a closed-aperture designates the closed-aperture (CA) Z-scan mode [21]. The nonlinear refractive index ($n2$) is evaluated via Eq. 1. Consequently, the real part of the third-order nonlinear susceptibility (Re(χ3)) is calculated using Eq. 2;

$$n_2 = \frac{\Delta \emptyset_0}{I_0 \, L_{eff} K} \tag{1}$$

$$R_e(\chi 3)(e.s.u) = 10^{-4} \, \frac{\varepsilon_0 \, n_0^2 \, c^2}{\pi} n_2 \tag{2}$$

where $I_0=2P/\pi\omega_0$ is the on-axis peak intensity at the focus, P represents the laser power, $K=2\pi/\lambda$ is the wave number $\Delta\emptyset_0$, is the nonlinear phase shift, $L_{eff}=1-e^{-\alpha_0 L}/\alpha_0$ is the effective length of the sample, L is the physical sample length, and α_0 is the linear absorption coefficient.

MATERIALS AND METHODS

The samples were synthesized via PLAL using deionized water (n=1.33). A Nd:YAG laser was used in the synthesis of nanoparticle samples, operating at wavelength of 1064 nm, a pulse energy of 120 mJ, and a repetition rate of 10 Hz with a pulse width of 5 ns. Two sets of nanoparticles were synthesized. The first group

contains bare metal nanoparticles including iron (Fe), copper (Cu), nickel (Ni), and cobalt (Co), each synthesized under laser irradiation for 4 minutes. The second group includes three samples of core/shell nanostructures (Fe@Cu, Fe@Ni, and Fe@Co). They are synthesized in a two-step sequential process: first, the core is created within 4 minutes, followed by the synthesis of the shell using the same aqueous solution for a variable duration of 2-4 minutes.

To evaluate the role of the shell in improving both linear and nonlinear optical properties, the formation of these samples was initially tracked by visual color changes in the aqueous solutions and subsequently confirmed via UV-Vis absorbance spectroscopy, the images of colloidal samples are illustrated in detail in Fig. 1a. The optical properties of the prepared nanostructures samples were characterized via UV-Vis spectroscopy. Additionally, Field Emission Scanning Electron Microscopy (FE-SEM, model JSM-7610F) was employed to determine and evaluate the morphology, with a focus on nanoparticles dimensions and geometry. As well as structural properties of samples were examined using a diffractometer (X-ray Diffraction (XRD) model D8 Advance, Bruker, Germany).

To evaluate the influence coating the iron NPs with a copper, nickel, and cobalt shell, which is expected to enhance both the linear and nonlinear optical properties, a Z-scan technique were utilized. The Z-scan operates with a continuous wave (CW) laser at a wavelength of 532 nm and a

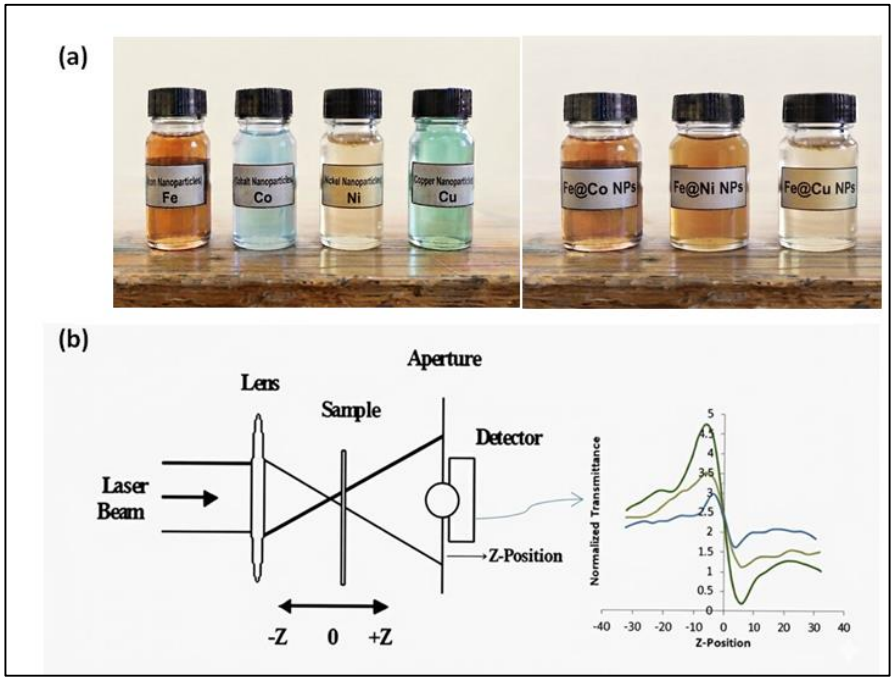

Fig. 1. Illustration of the experimental configurations (a) the images of colloidal samples, and (b) Z-Scan measurement system.

Table 1. The absorption peak position of the metallic nanoparticles.

Samples	Absorbance position (nm)
Fe NPs	387
Co NPs	380
Ni NPs	395
Cu NPs	570

power of 120 mW. The laser beam passes through a 1 mm quartz cell containing the sample, and the laser signal passes through the sample is then detected by a photodetector. The Z-scan technique (model-VER-8: MAHFANAVAR) utilized to evaluate the nonlinear optical properties of samples. The closed-aperture Z-scan configuration, as depicted in Fig. 1b, which is method exhibits simplicity and high sensitivity for analysis of nonlinear optical properties both bare and core/shell NPs. The Gaussian laser beam was centered using a convex lens (focal length of 20 cm) onto the samples. The transmitted beam power was recorded behind the aperture as a function of the sample position (z). The transmission spectrum and the signal reaching the detector were constantly tracked; the peak-to-valley transmittance change (ΔT_{p-v}) acts to directly evaluate the nonlinear parameters.

A standard Z-scan curve displaying a peak followed by a valley denotes a negative nonlinear refractive index ($n_2 < 0$). In this case, as the sample moves before the focal point ($z < 0$), self-defocusing arises, caused by the formation of a negative lens effect that reduces the detector signal. In contrast, an inverse Z-scan signature (a valley followed by a peak) represents a positive nonlinear refractive index ($n_2 > 0$). This behavior appears when the sample is positioned behind the focus ($z > 0$), where self-focusing create a positive lens effect, thereby increasing the detected signal intensity. Therefore, these measurements clarify the manifest contributions of self-focusing, self-defocusing, and self-phase modulation on the specific variation of the n_2 [22].

RESULTS AND DISCUSSION

The UV-Vis absorption spectra of the metallic NPs, displaying the intensity and position of the absorbance, are shown in Fig. 2.

It is observed from the absorption spectra of metallic NPs that Fe, Co, and Ni, which possess magnetic properties, have absorption peaks in the ultraviolet region of the electromagnetic spectrum and close to the visible region.

The position of these peaks depends on the size and shape of the metallic NPs, as well

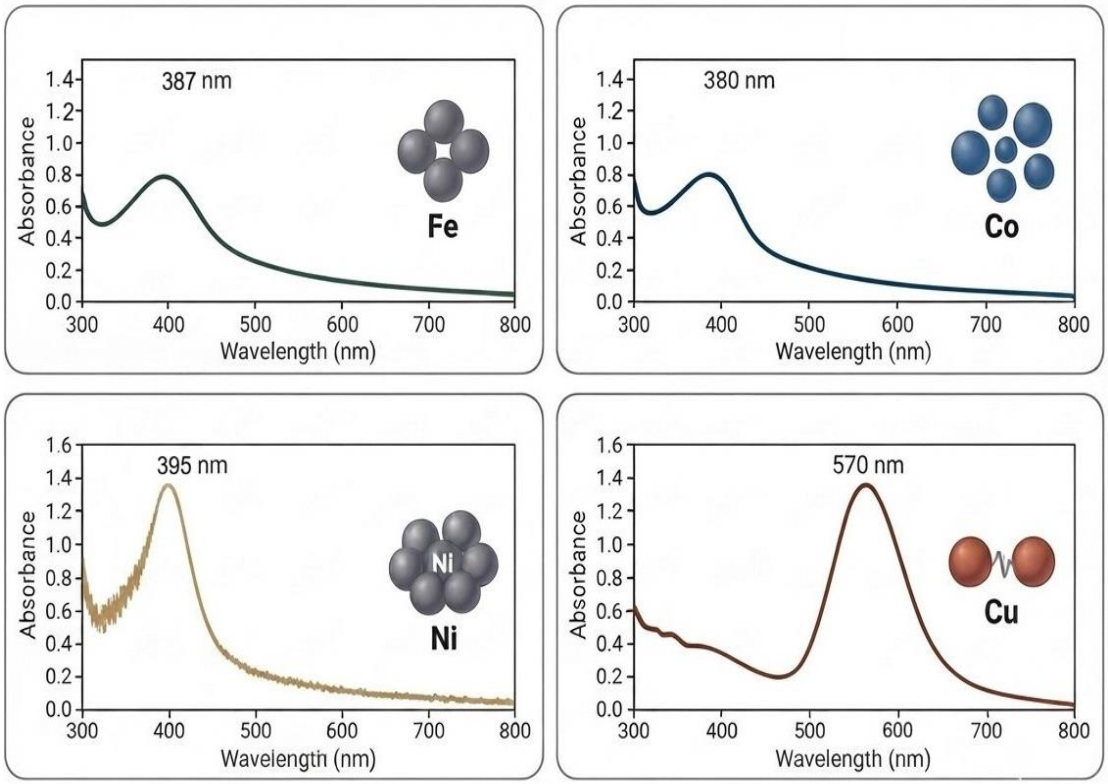

Fig. 2. The absorbance spectra of the metallic NPs.

as the refractive index of the surrounding environment. While Cu NPs exhibits a clear and distinct absorption peak at a wavelength of 570 nanometers, it is a plasmonic metal that reacts strongly with light passing through it. The positions of these absorption peaks are summarized in Table 1.

For the core/shell nanostructure samples, their absorption spectra are shown in Fig. 3, it is clearly observed that the absorbance value increases

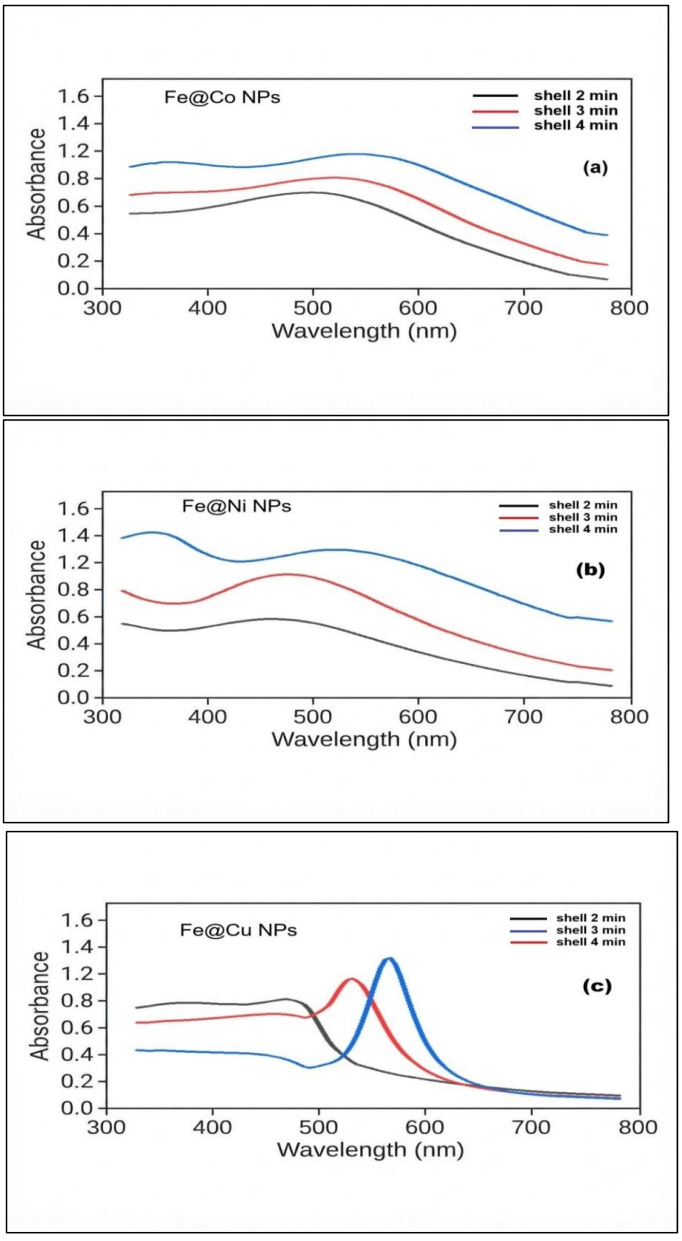

Fig. 3. The absorbance spectra of the core/shell NPs at a constant core growth time of 4 min, and a variable shell growth time of 2-4 min for (a) Fe@Co NPs, (b) Fe@Ni NPs, and (c) Fe@Cu NPs.

as the growth time of the shelling increases 2-4 min. This usually indicates an increase in the concentration of nanoparticles or an increase in their size as a result of the continued growth of the cobalt layer around the iron core over time, as shown in Fig. 3a.

The peaks observed in the absorption spectra indicate the interaction of light with free electrons on the surface of the Fe@Co nanostructures. It can also be observed that the absorption peak is not fixed in place but appears to shift slightly towards longer wavelengths (redshift) as the shell formation time increases.

This redshift is direct evidence of a change in the size of the Fe@Co nanostructures (i.e., an increase in the thickness of the cobalt shell), since an increase in shell thickness leads to a change in the frequency at which the surface electrons oscillate.

Fig. 3b shows the optical absorption spectral of the Fe@Ni nanostructures, i.e., an iron (Fe) core coated with a layer of nickel (Ni) as a shell, at different coating of growth times (2-4 min). The results show a direct increase in absorption intensity as the growth time of the nickel layer increases, indicating an increase in the size or density of the nanoparticles in solution as the reaction time continues. A major absorption peak is also observed for each curve, and this peak clearly shifts towards longer wavelengths (red shift) as the shell formation time increases. This shift in peak position is a direct result of the change in the thickness of the nickel shell around the iron nucleus, which enhances the magnetic properties of the iron, reduces its oxidation, and protects it from external conditions. Remarkably, a striking change in the absorption behavior of Fe@Cu nanostructures is evident, as shown in Fig. 3c.

This Figure demonstrates a significant shift in the position and shape of the SPR peak relative to the previous Figures (Fe@Ni and Fe@Co). For the black line (2 min), the peak appears low-intensity and relatively flat at short wavelengths. As the synthesis duration increases (red line for 3 min and blue line for 4 min), a very sharp and distinct absorption peak appears and shifts significantly towards longer wavelengths (red shift). This signifies the formation of a Cu shell. The sharp shift of the peak towards longer wavelengths (from about 500 nm to approximately 570 nm) clearly reflects the successful formation of the Cu shell around the Fe core.

The copper is known for its distinctive plasmonic properties in the visible spectrum, and the continued growth of this shell enhances the absorption intensity and shifts it towards the red end, indicating an increase in the thickness or uniformity of the copper layer.

Comparing the three nanostructures in the figure above reveals that, unlike the Fe@Co and Fe@Ni nanostructures which exhibited gradual increases in absorption, the Fe@Cu nanostructures show a more pronounced and specific plasmonic response as the shell time increases. This suggests

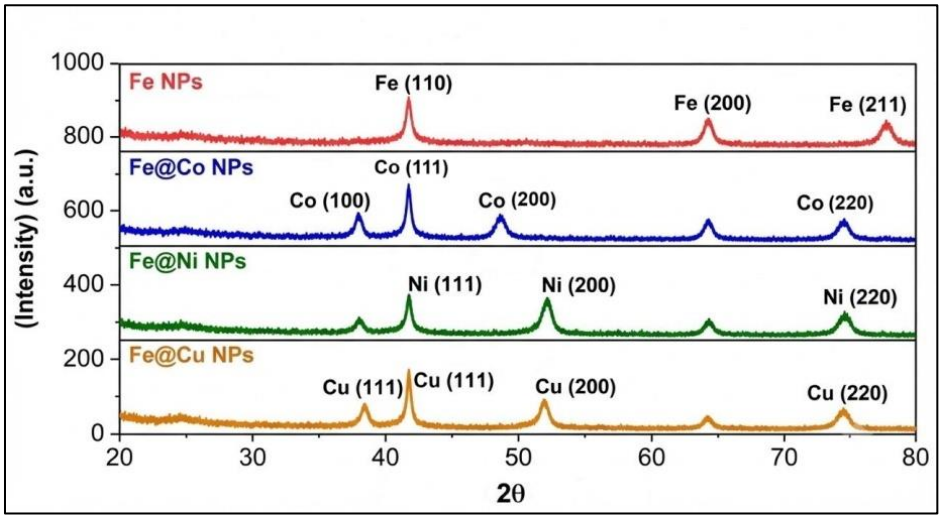

Fig. 4. XRD patterns of the Fe NPs and core/shell nanostructures.

that the growth of copper on the iron nucleus in this study resulted in clearer and more distinct optical properties in the plasmonic resonance range.

X-ray diffraction (XRD) provides an accurate characterization of nanoparticles, providing precise information about the crystal structure and purity of the metallic material, and also provides information about the non-oxidation of the nano-metals. Based on the XRD results of Fe NPs, it was found that the Fe NPs are in a pure metallic phase and no oxidation has occurred in the metal. This is

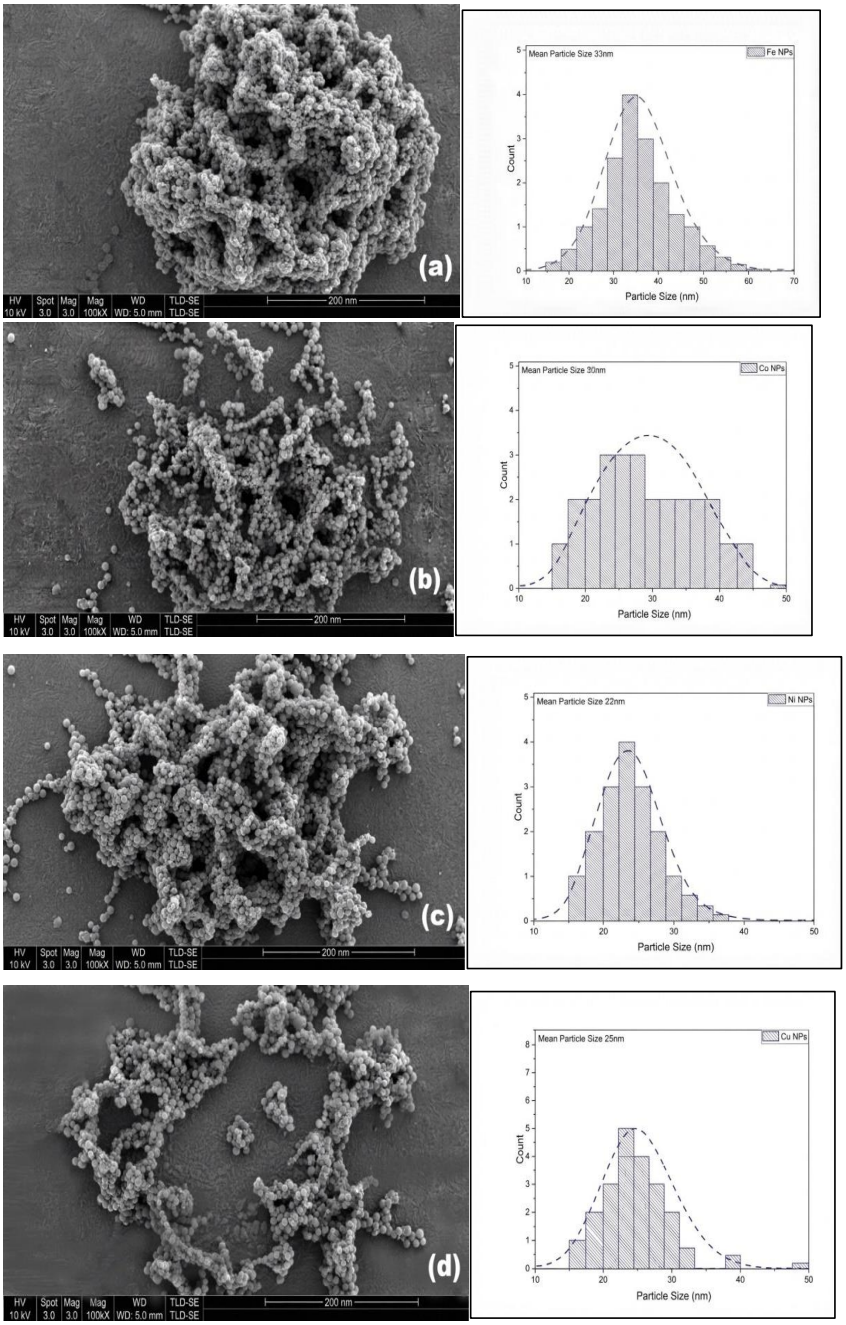

Fig. 5. FE-SEM images of metal samples in the left column, and histogram of particle size distribution in the right column of ; (a) Fe NPs, (b) Co NPs, (c) Ni NPs, and (d) Cu NPs.

observed from the diffraction peaks shown in Fig. 4, it diffraction patterns are observed, the peaks of which are usually at angles (2θ) characteristic of the body-centered cubic (BCC) crystal structure, where the main peak of Fe NPs is often 43°, and there are other less intense peaks at angles of 65° and 78°, This is clear evidence that Fe NPs do not oxidize. For core/shell nanostructures, the XRD spectrum of Fe@Co nanostructures exhibits a blended appearance, combining the crystalline properties of both metals, with minimal influence from surface overlap or lattice strain between the core and shell. Since iron, cobalt, and nickel all crystallize in cubic systems in their metallic phases, the peaks will overlap closely.

The above figure shows the appearance of

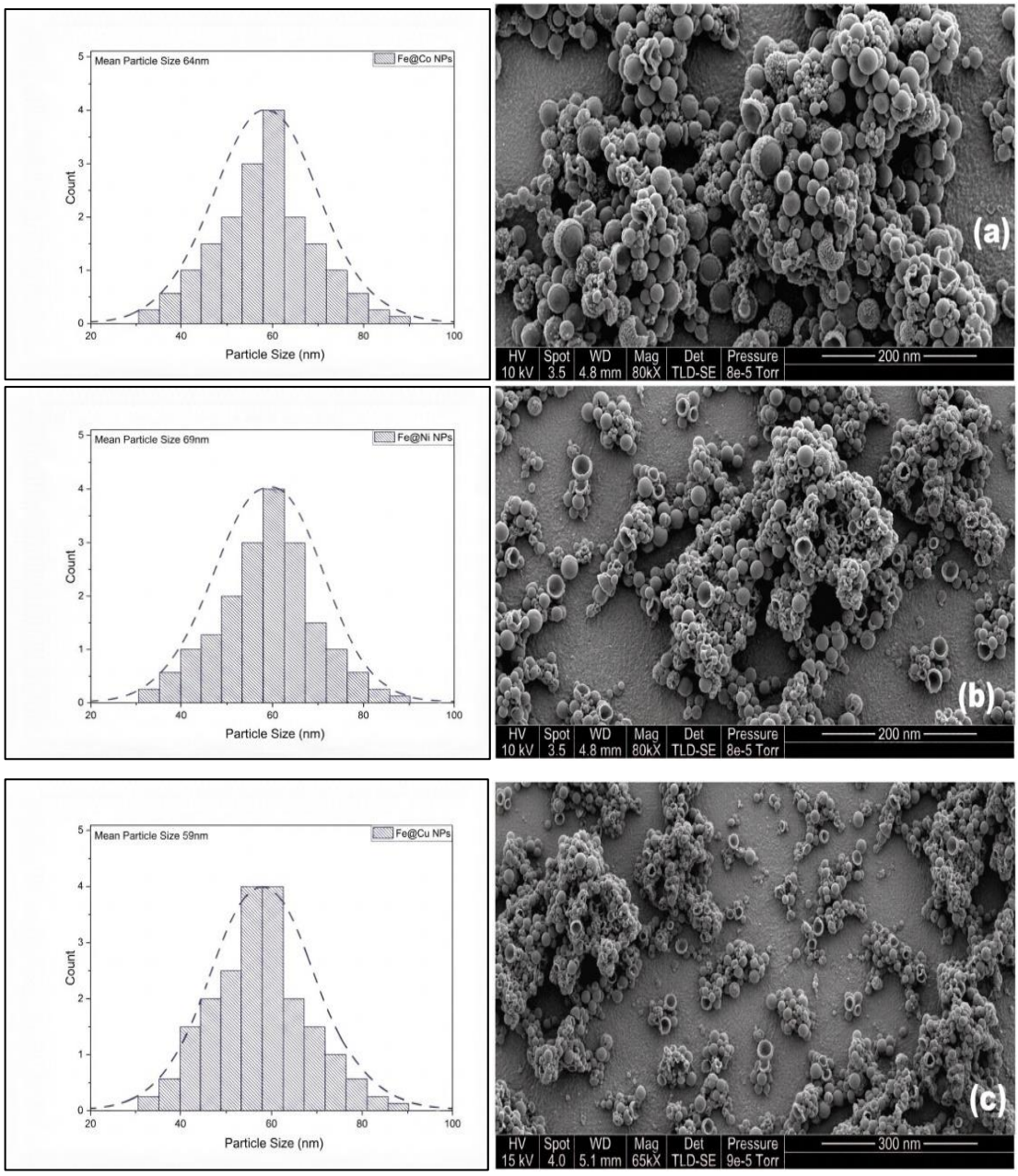

Fig. 6. FE-SEM images of core/shell samples in the right column, and histogram of particle size distribution in the left column of ; (a) Fe@Co NPs, (b) Fe@Ni NPs, and (c) Fe@Cu NPs.

a very strong peak at angle of 44° representing the crystalline levels (110) for iron (BCC-Fe) and level (111) for cobalt (FCC-Co) for the Fe@Co nanostructures. A diffraction peak appears at the 49° angle representing level (200) for cobalt (FCC), another peak at the 65° angle representing level (200) for iron (BCC), and a peak at the 76° angle representing level (220) for both iron and cobalt.

Similarly, Fe@Ni nanostructures are considered systems whose analysis relies on crystal interference, since both Fe and Ni have very close cubic crystal phases. In the XRD spectrum of Fe@Ni nanostructures, peaks are observed where the signals of iron (BCC) and nickel (FCC) interfere.

The results show that the main peak (43°- 44° region) in this area exhibits strong interference. The iron (110) peak for the BCC structure appears at approximately 43.1°, and the nickel (111) peak for the FCC structure appears at approximately 44.5°. In nanoscale samples, a single, very broad peak is typically observed, encompassing the contributions of both metals. The second peak (51°–52° region) in this area is primarily associated with nickel (200) and appears at approximately 51.8°. If the Ni shell is very thin, this peak may be weak or significantly broad. The additional iron peak (region 65°) shows the iron (200) peak of the BCC structure. The presence of this peak is a good indicator of the presence of an iron nucleus. The third nickel peak (region 75°) shows the nickel (220) peak of the FCC structure.

On the other hand, in Fe@Cu nanostructures, the XRD spectrum exhibits an interaction between the iron (BCC) and copper (FCC) crystal structures. Due to the lack of symmetry in their crystal systems, the spectrum is more distinct compared to Fe@Ni or Fe@Co nanostructures.

The peaks overlap considerably in Fe@Cu nanostructures, the main iron peak (44.7°) and the main copper peak (43.3°) appear as separate or very close peaks (appearing as a blended peak). Because the lattice constants differ significantly between copper and iron, a slight shift in the peak angles compared to the reference values may be observed, which is expected due to the mechanical stress at the core-shell interface. The copper peaks

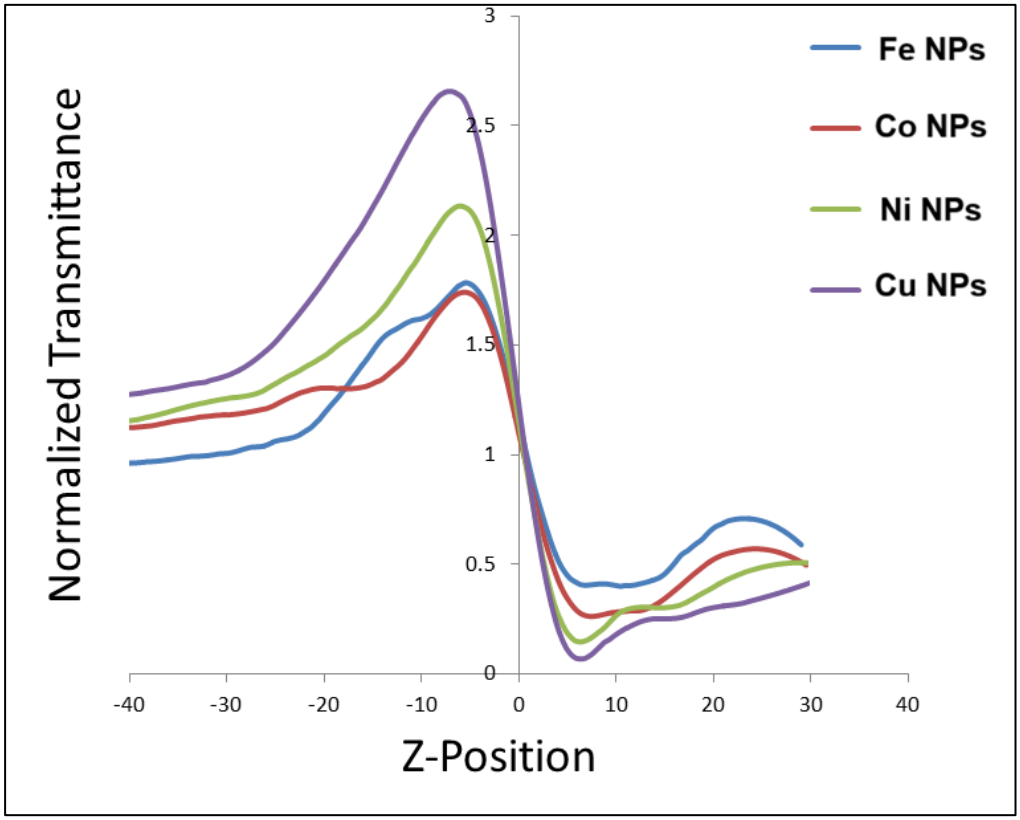

Fig. 7. Z-scan transmittance spectra of the metal NP samples under laser irradiation at wavelength of 532 nm.

(FCC shell) at angle 43.3° represent the (111) level of copper, at angle 51.4° it represent the (200) level of copper, and at angle 74.1° it represent the (220) level of copper.

A morphology of the samples are studied to determine the nanoparticles and core/shell nanostructures, a results morphology investigated using field emission scanning electron microscopy (FE-SEM) image, also the average size and average diameter calculated by software Image J.

Based on the results, FE-SEM images showed that the metal samples used in the study were spherical and semi-spherical, with an average size of 33 nm for Fe NPs, 30 nm for Co NPs, 22 nm for Ni NPs, and 25 nm for Cu NPs, as shown in Fig. 5.

The size variations of the spherical nanoparticles are very important in nano-photonic applications. the metal NPs with a size of 20 nm are suitable for biosensors and biological devices for disease detection and treatment, as their small size allows for increased surface interaction with the surrounding environment [23]. Similarly, metallic nanoparticles with a size of approximately 40 nm can combine chemical stability with the ability to generate catalytic properties, making them suitable for manufacturing electronic and optical devices [23]. The metallic nanoparticles with a size of 60 nm or larger are used to enhance solar cells or light-dependent electronics[24].

Meanwhile, the FE-SEM results of core/shell samples showed that successfully formed the clearly and distinctly, as in Fig. 6. As well as the results are showed that A significant increase in the size of the nanostructures compared to the bare metal nanoparticles in the previous Figure.

The average size of the nanostructures was found to be 64 nm for Fe@Co, 69 nm for Fe@Ni, and 59 nm for Fe@Cu. These values of 59-69 nm reflect an increase in nanoparticle diameter compared to the previous metal samples, which had an average diameter of 22-33 nm. This is expected when constructing core/shell nanostructures or coating nanometals around an iron core. These data are an excellent indicator of the success of the core/shell nanostructures, as the stability of the sizes around these values indicates the homogeneity of the prepared samples.

The Z-scan technique was employed to measure

Table 2. The nonlinear optical parameters measured of the metal NP samples under laser irradiation at wavelength of 532 nm.

Samples	Nonlinear parameters	
	n_2 (m^2/W) $\times 10^{-12}$	Re(χ3) × (e.s.u)10^{-6}
Fe NPs	-5.88	5.15
Co NPs	-4.27	3.96
Ni NPs	-6.67	6.29
Cu NPs	-9.38	9.41

Table 3. The nonlinear optical parameters measured of the core/shell nanostructure samples under laser irradiation at wavelength of 532 nm.

Samples	Nonlinear parameters	
	n_2 (m^2/W) $\times 10^{-12}$	Re(χ3) × (e.s.u)10^{-6}
Fe@Co NPs	-9.86	7.75
Fe@Ni NPs	-10.24	9.36
Fe@Cu NPs	-16.45	14.34

the nonlinear refractive index (n_2), and the real part of third-order nonlinear optical susceptibilities Re($\chi 3$) for all investigated samples. Fig. 7, illustrates the Z-scan normalized transmittance spectra (peak-to-valley transmittance ΔT_{p-v}) of the metals NP obtained under laser excitation at wavelengths of 532nm.

The variations in the n_2 and Re($\chi 3$) were

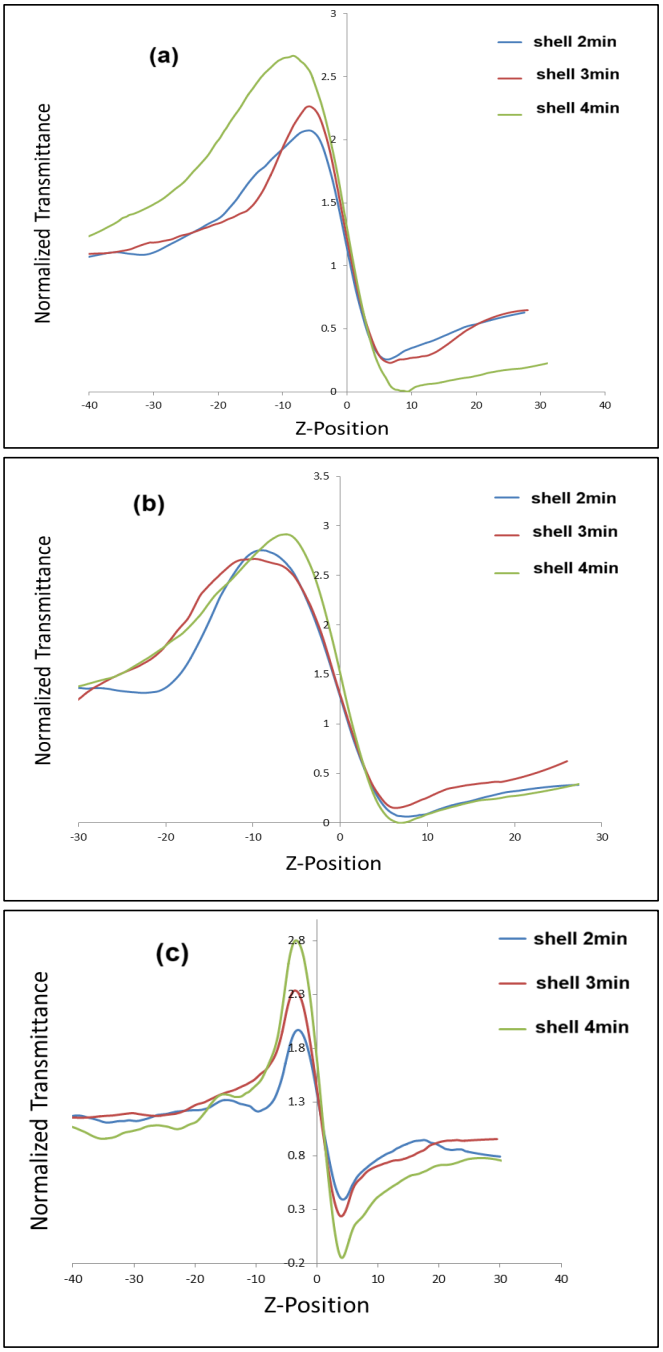

Fig. 8. Z-scan transmittance spectra of the core/shell nanostructure samples under laser irradiation at wavelength 532 nm with difference in shell time of; (a) Fe@Co, (b) Fe@Ni, and (c) Fe@Cu nanostructures.

evaluated based on the difference between ΔTp-v from the respective transmittance curves. The results show that the choice of laser excitation wavelength directly modifies the nonlinearity of the samples, This is clearly evident from the fractional changes demonstrated by these measured parameters. The calculated nonlinear optical parameters are summarized in Table 2.

Based on the results of the closed aperture Z-scan measurements, the spectra of normalized transmittance for all bare NP samples exhibit a characteristics peak-to-valley pattern, which confirms a negative nonlinear refractive index (n_2< 0). This self-defocusing behavior is considerably enhanced near the LSPR wavelengths of the plasmonic metal NPs, specifically since Cu NPs are a plasmonic material with an absorption spectrum close to the wavelength used for excitation, they exhibit higher nonlinearity coefficients compared to samples of other metals. Various physical mechanisms, including nonlinear scattering, electronic polarization, thermal effects, and molecular reorientation, contribute to this third-order optical nonlinearity [25]. Upon plasmonic excitation, the localized electric field is strongly enhanced in the vicinity of the metallic nanostructures, thus leading to a noticeable improvement in their resonant peaks.

With respect to the core/shell nanostructures, they similarly manifest a negative nonlinear refractive index, as illustrated by the behavior of the nonlinear transmittance curve in Fig. 8. The experimental findings confirm that the excitation laser wavelength directly controls the magnitude of the nonlinear optical parameters. Importantly, excitation at the surface plasmonic resonance wavelength of the Fe@Cu nanostructure induces a pronounced enhancement in the nonlinearity compared to the Fe@Ni, and Fe@Co nanostructures, as systematically summarized in Table 3.

The laser wavelength, which determines the excitation frequency in the Z-scan technique, closely matches the LSPR frequency of the plasmonic nanometals within the core/shell nanostructures. This resonance induces additional light absorption in the shell layer, inducing two types of electronic transitions: an inter-band transition between filled states in the conduction band and empty states, and an intra-band transition between the localized d-band and free electrons in the conduction bands [26]. Consequently, this enhances the optical nonlinearity of the system. This enhancement is primarily attributed to the electronic transitions from the conduction band of semiconductors to the localized surface plasmon level of the core/shell nanostructures [27].

The results indicate that the nonlinear properties of the core/shell nanostructure samples are significantly stronger than those of the metal NP samples. Specifically, the refractive index of the core/shell nanostructure samples is two or three times higher than that of the bare metal NPs. Noticeable nonlinearity in the core/shell nanostructure samples can be attributed to the thermal processes, a phenomenon common in nanomaterials under CW laser excitation. Such large nonlinear coefficients highlight the potential of the proposed nano-systems for applications in photo-electronic devices [28].

The thermal lens phenomenon a significant impact on this system due to the intensity dependent variation in the refractive index. Particularly, the medium acts as a negative lens, characterized by a lower refractive index at the center that increases towards the periphery. As the laser beam interacts with the sample, the phenomenon of thermal lens induces an additional phase shift in the propagating beam [25].

CONCLUSION

The overarching finding of this study demonstrates that the optical, structural, and environmental characteristics of core/shell Fe@Metal (Ni, Co, and Cu) nanostructures synthesized efficiently via PLAL technique are profoundly governed by both the choice of shell material and the duration of shell deposition. Specifically, adjusting shell growth parameters and utilizing metal such as nickel, cobalt, and copper effectively modulates SPR, induces characteristic spectral shifts, and significantly enhances nonlinear optical properties and crystal lattice compatibility. Furthermore, the quantitative evaluation revealed that the nonlinear parameters were substantially enhanced by two to three-fold. Optimizing shell thickness functions as a robust protective shield that prevents core oxidation, reduces environmental degradation, and curtails agglomeration. Consequently, these accurately designed core/shell nanostructures exhibit chemical and thermal stability, paving the way for advanced technological implementations in nanoelectronics, optical sensing, and specialized

optical devices.

CONFLICT OF INTEREST

The authors declare that there is no conflict of interests regarding the publication of this manuscript.

REFERENCES

1. Optical Properties of Metal Oxide Nanomaterials. Optical Properties and Spectroscopy of Nanomaterials: WORLD SCIENTIFIC; 2009. p. 181-203.
2. Albu A-M, Marian Târpă V. Polymer Architectures for Optical and Photonic Applications. Nonlinear Optics - Nonlinear Nanophotonics and Novel Materials for Nonlinear Optics: IntechOpen; 2022.
3. Ganeev RA. Low-order nonlinear optical properties of metal nanoparticles. Nanostructured Nonlinear Optical Materials: Elsevier; 2018. p. 117-163.
4. Stepanov AL. Nonlinear Optical Properties of Metal Nanoparticles in Silicate Glass. Glass Nanocomposites: Elsevier; 2016. p. 165-179.
5. Mbarak H, Kodeary AK, Hamidi SM, Mohajarani E, Zaatar Y. Control of nonlinear refractive index of AuNPs doped with nematic liquid crystal under external electric field. Optik. 2019;198:163299.
6. Review for "Multifunctional Lanthanide-Based Iron Oxide Luminescent Magnetic Nanoparticles: Synthesis, Properties and Biomedical Applications". Royal Society of Chemistry (RSC); 2026.
7. Decision letter for "Multifunctional Lanthanide-Based Iron Oxide Luminescent Magnetic Nanoparticles: Synthesis, Properties and Biomedical Applications". Royal Society of Chemistry (RSC); 2026.
8. Hastak V, Bandi S, Srivastav AK. Magnetic Iron Oxide Nanoparticles for Biomedical Applications. Advanced Materials for Biomechanical Applications: CRC Press; 2022. p. 85-111.
9. Zhang J, Tang Y, Weng L, Ouyang M. Versatile Strategy for Precisely Tailored Core@Shell Nanostructures with Single Shell Layer Accuracy: The Case of Metallic Shell. Nano Lett. 2009;9(12):4061-4065.
10. Kumar P, Kim K-H, Bansal V, Kumar N, Bhaskarwar AN. Core–shell nanostructures as a platform for sensing applications. Metal Semiconductor Core-Shell Nanostructures for Energy and Environmental Applications: Elsevier; 2017. p. 179-196.
11. Ejbarah RA, Kodeary AK, Abbas TM, Hamidi SM. Magneto - Plasmonic Properties of Hybrid Nanostructures Prepared by Laser Ablation in Different Solutions. Elsevier BV; 2023.
12. Pankaj P, Bhattacharya S, Chatterjee S. Competition of Core-Shell and Janus Morphology in Bimetallic Nanoparticles: Insights From a Phase-Field Model. Elsevier BV; 2021.
13. Karwi ZLI, Kodeary AK, Babaei F. Investigated numerically nanoshell thickness on photothermal response of hybrid nanostructures in an aqueous medium. Optik. 2024;313:172007.
14. Csiszár G, Solodenko H, Lawitzki R, Ma W, Everett C, Csiszár O. Nonlinear elastic aspects of multi-component iron oxide core–shell nanowires by means of atom probe tomography, analytical microscopy, and nonlinear mechanics. Nanoscale Advances. 2020;2(12):5710-5727.
15. Wurster B, Grumelli D, Hötger D, Gutzler R, Kern K. Driving the Oxygen Evolution Reaction by Nonlinear Cooperativity in Bimetallic Coordination Catalysts. Journal of the American Chemical Society. 2016;138(11):3623-3626.
16. Shi RP, Wang CP, Wheeler D, Liu XJ, Wang Y. Formation mechanisms of self-organized core/shell and core/shell/corona microstructures in liquid droplets of immiscible alloys. Acta Mater. 2013;61(4):1229-1243.
17. Guirado-López RA, Aguilera-Granja F. Bimetallic Fe−Ni Cluster Alloys: Stability of Core(Fe)−Shell(Ni) Arrays and Their Role Played in the Structure and Magnetic Behavior. The Journal of Physical Chemistry C. 2008;112(17):6729-6739.
18. Kodeary AK, Hamidi SM, Moradlou R. Voltage controlled properties of piezo-magneto-plasmonic core/shell nanoparticles. Nano-Structures and Nano-Objects. 2020;21:100415.
19. Rudenko V, Styopkin V, Liakhovetskyi V, Brodin A. Tunable third-order optical nonlinearity in Ag/Au nanostructures with Al_2O_3 coating layer under femtosecond and nanosecond excitation. Applied Nanoscience. 2025;16(1).
20. Kodeary AK, Hamidi SM. Tunable Piezophotonic Effect on Core-Shell Nanoparticles Prepared by Laser Ablation in Liquids under External Voltage. Journal of Nanotechnology. 2019;2019:1-11.
21. Mostafa AM, Mwafy EA, Awwad NS, Ibrahium HA. Au@Ag core/shell nanoparticles prepared by laser-assisted method for optical limiting applications. Journal of Materials Science: Materials in Electronics. 2021;32(11):14728-14739.
22. Henari FZ, Al-Saie A. Nonlinear refractive index measurements and self-action effects in Roselle-Hibiscus Sabdariffa solutions. Laser Physics. 2006;16(12):1664-1667.
23. Leelawattananon T, Chittayasothorn S. Simulation Effects on the Optical Response of Gold Nanoparticles. Proceedings of the 9th International Conference on Simulation and Modeling Methodologies, Technologies and Applications: SCITEPRESS - Science and Technology Publications; 2019. p. 360-367.
24. Chander N, Khan AF, Thouti E, Sardana SK, Chandrasekhar PS, Dutta V, et al. Size and concentration effects of gold nanoparticles on optical and electrical properties of plasmonic dye sensitized solar cells. Solar Energy. 2014;109:11-23.
25. E S, T A, D NR, K C. Nonlinear optical behavior of Au@Ag core- shell nanostructures. J Mol Liq. 2021;333:115935.
26. Mostafa AM, Mwafy EA, Awwad NS, Ibrahium HA. Catalytic activity of Ag nanoparticles and Au/Ag nanocomposite prepared by pulsed laser ablation technique against 4-nitrophenol for environmental applications. Journal of Materials Science: Materials in Electronics. 2021;32(9):11978-11988.
27. Saimon JA, Salim ET, Amin MH, Fakhri MA, Azzahrani AS, Ali ABM, et al. Ag@WO3 core–shell nanocomposite for wide range photo detection. Sci Rep. 2024;14(1).
28. Han W, Wang W, Fan J, Jia R, Yang X, Wu T, et al. A novel Ag/ZnO core–shell structure for efficient sterilization synergizing antibiotics and subsequently removing residuals. Green Energy and Environment. 2024;9(2):366-377.